The impact of aerosols on photolysis frequencies and ozone production in urban Beijing during the four-year period 2012–2015

Wenjie Wang[1], Min Shao[1,2*], Min Hu[1], Limin Zeng[1], YushengWu[1]

1 State Joint Key Laboratory of Environmental Simulation and Pollution Control, College of Environmental Sciences and Engineering, Peking University, Beijing 100871, China

2 Institute for Environmental and Climate Research, Jinan University, Guangzhou 511443, China

*** Correspondence to:**

Prof. Min SHAO

College of Environmental Sciences and Engineering, Peking University, Beijing 100871, China

Tel: +86-10-62757973; Fax: +86-10-62757973

Email: mshao@pku.edu.cn

Abstract

During the period 2012-2015, the photolysis frequencies were measured at the Peking University site (PKUERS), a representative site of urban Beijing. We present a study of the effects of aerosols on two key photolysis frequencies, $j(O^1D)$ and $j(NO_2)$. Both $j(O^1D)$ and $j(NO_2)$ display significant dependence on AOD with a nonlinear negative correlation. With the increase in AOD, the slopes of photolysis frequencies vs AOD decrease, which indicates that the capacity of aerosols to reduce the actinic flux decreases with AOD. In addition, the slopes are equal to $4.21\text{-}6.93\blacksquare10^{-6}$ s^{-1} and $3.20\blacksquare10^{-3}$ s^{-1}per AOD unit for $j(O^1D)$ and $j(NO_2)$ respectively at SZA of 60°, both of which are larger than those observed in the Mediterranean. This indicates that the aerosols in urban Beijing have a stronger extinction on actinic flux than absorptive dust aerosols in the Mediterranean. Since the photolysis frequencies strongly depended on the AOD and the solar zenith angle (SZA), we established a parametric equation to quantitatively evaluate the effect of aerosols on photolysis frequencies in Beijing. According to the parametric equation, aerosols lead to a decrease in $j(NO_2)$ by 24.2% and 30.4% for summer and winter, respectively, and the corresponding decrease in $j(O^1D)$ by 27.3% and 32.6% respectively, compared to an aerosol-free atmosphere. Based on an observation campaign in August 2012, we used the photochemical box model to simulate the ozone production rate ($P(O_3)$). The simulation results shows that the monthly average net ozone production rate is reduced by up to 25% due to the light extinction of aerosols. Through further in-depth analysis, it was found that particulate matter concentrations maintain high level under

the condition of high concentrations of ozone precursors (VOCs and NOx), which inhibits the production of ozone to a large extent. This phenomenon implies a negative feedback mechanism in the atmospheric environment of urban Beijing.

1. Introduction

Solar radiation plays an important role in atmospheric photochemistry, driving the photolysis of many key species. The photolysis of ozone (O_3), gaseous nitrous acid (HONO), and carbonyl species, which contributes to the primary production of HOx (Volkamer et al., 2010). The photolysis of ozone produces O^1D, which then reacts with H_2O to form OH radicals; these radicals are the main source of OH radicals in the troposphere, as shown by reactions R1 and R2. The strong dependence of OH concentration on $j(O^1D)$ was found in a number of field measurements (Ehhalt et al., 2000; Rohrer et al., 2014; Stone et al., 2012). In addition, the photolysis of NO_2 produces O^3P, and then O^3P reacts with O_2 to produce O_3, as shown by reactions R3 and R4, which is the only significant source of ozone in the troposphere (Finlayson-Pitts et al., 2000). The photolysis frequencies of R1 and R3 are $j(O^1D)$ and $j(NO_2)$, respectively.

$$O_3 + h\nu \ (\lambda < 330\ nm) \rightarrow O^1D + O_2 \quad \text{(R1)}$$

$$O^1D + H_2O \rightarrow 2OH \quad \text{(R2)}$$

$$NO_2 + h\nu \ (\lambda < 430\ nm) \rightarrow NO + O(^3P) \quad \text{(R3)}$$

$$O\left(^3P\right) + O_2 \rightarrow O_3 \quad \text{(R4)}$$

The photolysis frequencies are calculated by the following formula:

$$j = \int_{\lambda_1}^{\lambda_2} F(\lambda)\sigma(\lambda, S, T)\varphi(\lambda, S, T)\,\mathrm{d}\lambda \quad \text{(E1)}$$

F(λ) is the actinic flux dependent on wavelength. σ(λ, S, T) is the absorption cross section of the species that absorbs in the wavelength range λ_1-λ_2. φ(λ, S, T) is the quantum yield of the photodissociation reaction product. λ, S and T represent wavelength, species and temperature, respectively.

The effect of aerosols on photolysis frequencies depends on the aerosol optical properties, SZA and altitude (Liao et al., 1999). The aerosol optical depth (AOD) characterizes the integral of the extinction coefficient of aerosols in the vertical direction. The light extinction of aerosols includes scattering and absorption, which have different effects on the actinic flux. Scattering aerosols can enhance the actinic flux throughout the troposphere, while absorptive aerosols reduce the actinic flux throughout the boundary layer (Jacobson, 1998; Dickerson et al., 1997; Castro et al., 2001). To distinguish between these two components, single scattering albedo (SSA) is defined as the ratio of the scattering coefficient to the total extinction coefficient. In areas with severe aerosol pollution, aerosols can significantly affect photolysis frequencies and ozone production. Studies in Los Angeles (Jacobson, 1998), Mexico City (Castro et al., 2001; Raga et al., 2001; Li et al., 2011), São Paulo (de Miranda et al., 2005), Huston (Flynn et al., 2010), Europe (Real et al., 2011) and Russia (Pere et al., 2015) have found that aerosols reduce ozone concentration by 5-30% by attenuating photolysis frequencies. Studies in the eastern United States have shown

that scattering aerosols increase ozone concentration by 5-60% by increasing the photolysis frequencies (Dickerson et al., 1997; He and Carmichael, 1999). Therefore, it is necessary to quantitatively evaluate the effect of aerosols on photolysis frequencies for the purpose of effective ozone prevention.

Currently, the methods for quantitatively evaluating the influence of aerosols on photolysis frequencies mainly include radiative transfer model and parameterization method (Madronich et al., 1993). Radiative transfer model is based on an algorithm for calculating solar radiation and photolysis frequencies (Madronich et al., 1999). The observed data of related influential factors of the photolysis frequencies are taken as the model's input and the photolysis frequencies simulated are compared with the observed value to test the simulation effect. The method comprehensively considers the influence of aerosol optical properties on the photolysis frequencies, but it does not necessarily reflect the true quantitative relationship in the atmosphere due to complicated environmental conditions and thus the simulated results don't necessarily reproduce observed values well (Lefer et al., 2003; Shetter et al., 2003; Hofzumahaus et al., 2004). For example, the simulated slope of $j(O^1D)$ vs AOD by Fast-JX algorithm within the CHIMERE model was significantly smaller than the observed slope, particularly for the high SZA values (Mailler et al., 2016). The parameterization method is based on the observation data taken from a certain region and is used to establish the parameterized relationship between the photolysis frequencies and optical properties of aerosols (such as AOD). The method can reflect the actual atmospheric environment conditions; it also considers less influential factors and thus

is easy to apply (Casasanta et al., 2011; Gerasopoulos et al., 2012). The disadvantage of this method is that the established parametric equations apply only to a specific region and cannot be extended to other regions.

With rapid economic development and urbanization in past decades, China's atmospheric pollution has become more and more severe, characterized by high concentrations of particulate matter and ozone. Satellite observations indicates that both the particulate matter and the ozone of eastern China are at higher levels compared with other locations in the globe (Verstraeten et al., 2015; Ma et al., 2014). Levels of pollution in the Beijing–Tianjin–Hebei are even more severe (Chang et al., 2009; Che et al., 2008; Zhang et al., 2014, Zhang et al., 2016). Therefore, it is necessary to study the effects of aerosols on photolysis frequencies and ozone production in the urban areas of China.

Previous model studies have shown that aerosols in China can affect ozone production by changing the photolysis rate. Tang et al. (2004) used a sulfur transmission–emission model (STEM) to discover that ozone concentration in northeastern China was reduced by 0.1–0.8% in the sandstorm due to the change in photolysis rate. Tie et al. (2005) used a global aerosol–chemical model to show that aerosols caused $j(O^1D)$ and $j(NO_2)$ to decrease in winter by 20%-30% and 10%-30%, respectively, and in summer by 5%-20% and 1%-10%, respectively, resulting in 2%-5% and 2% reductions in ozone concentration in winter and summer, respectively. Li et al. (2011) used an air quality model to estimate the changes in the photolysis rate caused by sulfate, nitrate, ammonium, and mineral dust aerosols in the central and eastern

132 regions of China from June 1 to June 12, 2006. This study showed that the daily
133 average j(O^1D) in the troposphere at the altitude of 1 km, 3 km, and 10 km from the
134 ground was reduced by 53.3%, 37.2%, and 20.9%, respectively, resulting in a
135 decrease in the ozone concentration by 5.4%, 3.8%, and 0.1% in the three layers. Lou
136 et al (2014) found that with aerosols, annual mean photolysis rates, j(O^1D)) and
137 j(NO_2), were simulated to be reduced by 6-18% in polluted eastern China, leading to
138 reductions in O_3 of up to 0.5 ppbv in those regions in spring and summer by using the
139 global chemical transport model (GEOS-Chem). However, all of these studies base
140 their results on model simulations. Research using long-term observational data to
141 evaluate the effects of aerosols on photolysis frequencies and ozone production in
142 China has not yet been published.

143 Our overall goal is to quantitatively evaluate the effect of aerosols in urban
144 Beijing on photolysis frequencies and thus on ozone production. First, the relationship
145 between $PM_{2.5}$ and AOD was investigated. Second, based on long-term observations
146 (2012-2015) of photolysis frequencies, we discussed the impact of AOD on photolysis
147 frequencies (j(O^1D) and j(NO_2)) in urban Beijing in detail. Then, the quantitative
148 relationship between photolysis frequencies, AOD, and SZA was acquired by the
149 parameterization method, which could be used to quantitatively evaluate the effect of
150 AOD on photolysis frequencies in Beijing. Finally, a photochemistry box model was
151 used to evaluate the effect of aerosols on ozone production.

2. Methodology

2.1. Measurement

From 2012 to 2015, $j(O^1D)$ and $j(NO_2)$ were measured continuously at PKUERS site. The site (39.99°N, 116.31°E) is located on the sixth floor of a campus building at the Peking University, 20 km northwest of Tiananmen Square. The height from the ground is about 30 m. The sampling point is surrounded by classroom buildings. Concentration level and composition of air pollutants were thought to be similar to the downtown so as to be representative for the whole of Beijing (Wang et al., 2010; Xu et al., 2011; Zhang et al., 2012; Zhang et al., 2014).

The actinic flux was measured using a spectroradiometer and the photolysis frequencies were calculated from the absorption cross section and quantum yield of each species (Shetter and Muler, 1999). The spectroradiometer consisted of a single monochromator with a fixed grating (CARL ZEISS), an entrance optic with a 2π steradian (sr) solid angle quartz diffusor and a flexible optical quartz fiber bundle connecting both components. The spectral measurements were performed with a wavelength resolution of 2 nm, covering a wavelength range of 290-650 nm (Hofzumahaus et al., 1999). The measured spectra were corrected for dark signal and stray light. Descriptions of the calibration procedure and calculation of photolysis frequencies are given in Bohn et al.(2008). The calculated photolysis frequencies had a time resolution of 10 s and an uncertainty of ±10%.

The optical properties of aerosols were measured by a CIMEL solar photometer (AERONET level 2 data collection, http://aeronet.gsfc.nasa.gov/) and the site selected was the Beijing-CAMS site (39.933°N, 116.317°E), which is close to the PKUERS site. The CIMEL solar photometer is an automatic solar-sky scanning radiometer that uses selected spectral channels. The instrumentation, data acquisition, retrieval algorithms, and calibration procedure conform to the standards of the AERONET global network and have been described in detail by Fotiadi et al. (2006). The solar extinction measurement was performed every 3 minutes in the spectral range 340–1020 nm for the calculation of AOD at wavelengths 340, 380, 440, 500, 675, 870, 970, and 1020 nm. Under cloudless conditions, the overall uncertainty of AOD data is ± 1% at $\lambda > 440$ nm and ± 0.02 at shorter wavelengths. In this study, AOD at the wavelength of 380 nm was chosen for analysis. This wavelength was selected as it is more representative of $j(NO_2)$. The SSA data were derived from a field campaign undertaken in August 2012. The absorption and scattering coefficients were measured with an Aethalometer (AE-31, Magee) and a Single Wavelength Integrating Nephelometer (Aurora-1000), respectively, with a time resolution of 1 minute. Five-minute averages of ozone column concentration, SSA, and photolysis frequencies were analyzed in this study. The total ozone column was obtained by OMI (Ozone Monitoring Instrument) for the year 2012-2015, using overpass data.

The analysis of the effects of aerosols on ozone production (Section 3.4) was based on the field campaign undertaken in August 2012. The relevant contents and methods of observation are shown in Table 1. In addition, meteorological parameters

such as temperature, humidity, and pressure were simultaneously observed at the site. Since the time resolution of VOCs is 1 hour, all data analyzed in Section 3.4 was processed as 1-hour average values. In this study, we focused on the effects of aerosols on photolysis frequencies and ozone production under cloudless conditions.

2.2 Radiative Transfer Model Description

We use the Tropospheric Ultraviolet and Visible (TUV) radiation model provided by Sasha Madronich (Madronich, 1993). In order to solve the radiative transfer equation, TUV uses the discrete-ordinates algorithm (DISORT) with 16 streams and calculate the global irradiance spectra in 0.15 nm steps and resolution. The key aerosol optical properties including AOD, SSA and AE are input into the model to test the effect of aerosols on photolysis frequencies.

2.3 Photochemical box model

The photochemical box model used in this study is based on a regional atmospheric chemical mechanism (RACM2) described by Goliff et al. (2013). The mechanism includes 17 stable inorganic compounds, 4 intermediate inorganic compounds, 55 stable organic compounds, and 43 intermediate organic compounds. Compounds not specifically treated in RACM are incorporated into species with similar functional groups. The isoprene-related mechanism used in this model is LIM mechanism proposed by Peeters et al. (2009). In this study, the observed NO_2, CO, SO_2, C2–C12 NMHCs, HCHO, photolysis frequencies, temperature, pressure, and relative humidity were used as constraints to simulate the concentrations of reactive

radicals (RO_2, HO_2, and OH), intermediate species, and associated reaction rate constants. HONO wasn't measured during the period and was calculated according to the concentration of NO_2 and the observed ratio of HONO to NO_2 at an urban site in Beijing, which had a marked diurnal cycle, a maximum in the early morning (ratio values up to ~0.05–0.08 in summer) and a decrease during daytime to values around 0.01–0.02 (Hendrick et al., 2014). The model was spun up for two days once it started running in order to ensure that the simulation was stable. It was assumed that the lifetime of simulated species removed by dry deposit was 24 hours. The lifetime corresponds to the assumed deposit rate of 1.2 cm s^{-1} and a well-mixed boundary layer height of about 1 km (Lu et al., 2012). Net ozone production is equal to the reaction rate between peroxy radicals (RO_2 and HO_2) and NO minus the loss rate of NO_2 and O_3 as shown in E2, E3, and E4. The ozone production rate ($P(O_3)$), the ozone loss rate ($D(O_3)$), and the net $P(O_3)$ were calculated from the simulation results.

$$P(O_3) = k_{HO2+NO}[HO_2][NO] + \sum\left(k^i{}_{RO2+NO}\left[RO^i{}_2\right][NO]\right) \quad \text{(E2)}$$

$$D(O_3) = (\theta j(O^1D) + k_{OH+O3}[OH] + k_{HO2+O3}[HO_2] + \sum(k^j{}_{alkene+O3}[alkene^j]))[O_3] + k_{OH+NO2}[OH][NO_2] \quad \text{(E3)}$$

$$net\ P(O_3) = P(O_3) - D(O_3) \quad \text{(E4)}$$

3. Results and discussion

3.1 The correlation between $PM_{2.5}$ and AOD

In order to evaluate the extinction capacity of near-surface $PM_{2.5}$, we investigated the relationship between $PM_{2.5}$ and AOD (at 380nm). The factors that affect this relationship include aerosol type, aerosol size distribution, aerosol distribution in the vertical direction, relative humidity (RH) and planetary boundary layer height (PBLH) (van Donkelaar et al., 2010). Figure 1 shows the correlation between AOD and $PM_{2.5}$ in four different seasons. The determination coefficient (r^2) is 0.53, 0.58, 0.62 and 0.59 for spring (March, April and May), summer (June, July and August), autumn (September, October and November) and winter (December, January and February), respectively. Meanwhile, the correlation exhibits significant seasonal differences, having relatively smaller slope (23.56) in summer and relatively larger slope (73.76) in winter (Table 2). This implies that the aerosols in summer have stronger extinction capacity in summer than in winter. One reason for the seasonal differences is the variation in RH among different seasons. There is higher RH in summer (57.2% on average) than in winter (30.4% on average), leading to stronger hygroscopic growth of aerosol particles, and thus resulting in higher scattering ability of aerosol particles. According to another study in urban Beijing, the higher the RH, the smaller the slope, and the higher the PBLH, the smaller the slope. In addition, the slope was smaller for scattering-dominant aerosols than for absorbing-dominant

aerosols, and smaller for coarse mode aerosols than for fine mode aerosols (Zheng, C. W et al., 2017). The slopes of the correlation between AOD (at 550nm) and $PM_{2.5}$ in this study in summer and winter are equal to 42.2μg m^{-3} and 119.2μg m^{-3}, respectively, close to that from Ma et al. (2016) (54.9μg m^{-3} and 110.5μg m^{-3}) and Xin et al. (2016) (55.2 μg m^{-3} and 93.4μg m^{-3}), but smaller significantly than that from Zheng et al. (2017) (65~74μg m^{-3} and 143~158μg m^{-3}). The differences mainly depend on the aerosol composition and size distribution at different observational sites in Beijing. Compared with other cities in North China (Tianjin, Shijiazhuang and Baoding) (Ma et al., 2016), the slope in Beijing for winter is significantly higher, indicating that the extinction capacity of aerosols in Beijing is weaker in winter.

3.2 Seasonal and diurnal variability of AOD and photolysis frequencies

The diurnal cycles of AOD is shown in Figure 2. AOD displays obvious diurnal variation, with relatively high level at noon and low level at dawn and evening. The diurnal variation of $PM_{2.5}$ is opposite to AOD. The opposite diurnal variation of AOD and $PM_{2.5}$ is mainly due to higher development of planetary boundary layer at noon, resulting in more complete mixture of particulate matter in the vertical direction. In addition, AOD has obvious seasonal differences, with the highest AOD in summer and the lowest AOD in winter. Conversely, $PM_{2.5}$ in winter (66.9μg m^{-3}) is significantly higher than in summer (45.5μg m^{-3}). In spite of lower $PM_{2.5}$ in summer, AOD in summer is higher due to stronger extinction capacity of $PM_{2.5}$ as discussed in

3.1. Figure 3 shows the diurnal variation of the photolysis frequencies under cloudless conditions for each season. $j(O^1D)$ and $j(NO_2)$ are both highest in summer, followed by spring and autumn, and lowest in winter. This seasonal difference is mainly determined by the difference in SZA for the four seasons.

The observed photolysis frequencies at this site are lower than that observed in the eastern Mediterranean (Crete, Greece, 35°20′N,25°40′E) (Gerasopoulos et al., 2012) by 7.8×10^{-6} s^{-1} and 4.9×10^{-6} s^{-1} for $j(O^1D)$, and 1.9×10^{-3} s^{-1} and 3.3×10^{-3} s^{-1} for $j(NO_2)$, in summer and winter respectively. The corresponding lower photolysis frequencies of Beijing than the eastern Mediterranean due to SZA difference is 1.7×10^{-6} s^{-1} and 3.0×10^{-6} s^{-1} for $j(O^1D)$, and 8.0×10^{-5} s^{-1} and 6.6×10^{-4} s^{-1} for $j(NO_2)$ according to TUV model, which are significantly lower than observed decreased magnitudes. Taking into account the similar levels of ozone column concentration in the two sites, the large gap of photolysis frequencies in the two sites is mainly attributed to the higher AOD in Beijing (0.76 ± 0.75) than in the eastern Mediterranean (0.27 ± 0.13).

It can be seen from Figure 3 that the difference between winter and summer for $j(O^1D)$ is significantly larger than that for $j(NO_2)$, where the summer midday averages of $j(O^1D)$ and $j(NO_2)$ are 5 times and 2 times those of winter, respectively. There are two reasons for this phenomenon. One, compared with $j(NO_2)$, $j(O^1D)$ is more sensitive to the change in SZA and the same change in SZA results in a larger change in $j(O^1D)$ than $j(NO_2)$. Two, the main influential factors of $j(NO_2)$ under cloudless conditions are SZA and AOD, and the influence of ozone column concentration and

temperature on $j(NO_2)$ is negligible. However, $j(O^1D)$ is affected significantly by the ozone column concentration and temperature, in addition to SZA and AOD. The higher ozone column concentration and lower temperature in winter than in summer lead to the difference in $j(O^1D)$ further increasing.

3.3 The correlation between photolysis frequencies and AOD

3.3.1 The correlation between $j(O^1D)$ and AOD

In order to rule out the effect of SZA on photolysis frequencies, we chose SZA equal to 30° and 60° (± 1°) for analysis. Figure 4 presents the dependence of $j(O^1D)$ on AOD at different levels of ozone column concentration at SZA of 30° and 60° (± 1°). The ozone column concentration has a classification width of 30 DU. $j(O^1D)$ exhibits a clear dependence on AOD, with a nonlinear negative correlation. As AOD increased, the slope of $j(O^1D)$-AOD gradually decreases, indicating that the ability of aerosols to reduce $j(O^1D)$ gradually decreases with AOD. This result differs from that found in Mediterranean, where $j(O^1D)$ was linearly negatively correlated with AOD (Casasanta et al., 2011; Gerasopoulos., 2012). A larger variation range of AOD in Beijing (0-3) compared with Mediterranean (0-0.6) is one reason for the difference.

For further analysis, the observed relation between $j(O^1D)$ and AOD was compared with TUV-simulated results. Panels a and b of Figure 5 present the comparison between observed and TUV-simulated $j(O^1D)$ against AOD at a SZA of

30° and 60° respectively and ozone column concentration of 330-360 DU. At low AOD level (< 0.8), the observed slope of $j(O^1D)$ vs AOD is significantly larger than the simulated slope at SSA of 0.95, and slightly larger than the simulated slope at SSA of 0.85. With AOD increasing, the observed slope decreases rapidly to the level smaller than the simulated slopes. The rapid change of the slope with AOD can be related to the variation of SSA at different AOD level. Figure 6 presents the relationship between SSA and AOD based on observed data in August 2012. The result suggests a significant correlation between SSA and AOD. With the increase in AOD, SSA is elevated; meanwhile, the slope of SSA vs AOD is gradually reduced. SSA characterizes the ratio of the scattering extinction coefficient to the total extinction coefficient (scattering extinction coefficient plus absorptive extinction coefficient) of aerosols. The smaller the SSA, the higher the absorptive component and lower the scattering component of the aerosol, and the stronger the ability of the aerosol to reduce the actinic flux (Dickerson et al., 1997). Figure 6 indicates that aerosols in Beijing under low AOD conditions had a higher proportion of absorptive aerosol components than under high AOD conditions, and, as a result, had a stronger ability to reduce the photolysis frequencies, which contributed to the rapidly reduced slope of $j(O^1D)$ vs AOD with AOD. However, due to absence of more SSA data of the period 2012-2015, we can't give more sufficient evidence for the dependence of SSA on AOD. For another perspective, Owing to the biomass burning and soot emission generated from heating, the fine mode heavily-absorbing aerosol percentage is higher in winter than in summer (Zheng et al., 2017; Liu et al., 2016; Zhang et al., 2013), and

thus aerosols in winter have stronger ability to reduce the photolysis frequencies. High AOD levels often appeared in summer and low AOD levels occurred mostly in winter (Figure 2), another fact that may also explains the rapidly reduced slope of $j(O^1D)$ vs AOD with AOD.

Comparing panels a and b of Figure 4, we see that at AOD smaller than 1, the slope of $j(O^1D)$ vs AOD exhibits a significant dependence on SZA and the slope at 30° of SZA is about 1.5-2.0 times larger than that at 60° of SZA. This result is similar to that of the observations made in the central Mediterranean (Casasanta et al., 2011). For the purpose of comparison with the study in the Mediterranean, the slope of $j(O^1D)$ vs AOD was calculated at AOD smaller than 0.7.

Table 3 presents slope, intercept and the determination coefficient (r^2) of linear fits of correlation between $j(O^1D)$ and AOD for each ozone column class at AOD smaller than 0.7. At SZA of 60° and O_3 column concentration of 300-330 DU, the respective slope of the linear regression indicates a reduction of $j(O^1D)$ by $4.21 \cdot 10^{-6}$ s^{-1} per AOD unit. Gerasopoulos et al. (2012) reported that the observed slope in the eastern Mediterranean was equal to $2.44 \cdot 10^{-6}$ s^{-1} at O_3 column of 300-320 DU. Casasanta et al. (2011) reported that the observed slope in the central Mediterranean varied from $2.66 \cdot 10^{-6}$ s^{-1} to $3.87 \cdot 10^{-6}$ at O_3 column of 300-330 DU. All of these results are smaller than the value of the present study, indicating that aerosols in urban Beijing had a stronger extinction capacity on $j(O^1D)$ than those in the Mediterranean that was influenced by both natural absorptive aerosols and anthropogenic aerosols. Previous study indicated that SSA in Beijing ranged from 0.80 to 0.86 (Garland et al.,

2009;Han et al., 2015b; Han et al., 2017; Tian et al., 2015). The relatively low SSA in Beijing could be an important reason for the stronger extinction capacity.

3.3.2 The correlation between $j(NO_2)$ and AOD

Unlike $j(O^1D)$, $j(NO_2)$ is negligibly affected by ozone column concentration and depends mainly on AOD and SZA under cloudless conditions. Figure 7 presents the dependence of $j(NO_2)$ on AOD at different SZA levels under cloudless conditions. The cosine of SZA (cos (SZA)) is categorized according to a width of 0.2. In the same category of cos (SZA), $j(NO_2)$ displays a strong dependence on AOD. When cos(SZA) is at its maximum level (0.8–1), the correlation between $j(NO_2)$ and AOD is close to linear. When cos (SZA) decreases, the correlation tends to be nonlinear. Similar to $j(O^1D)$, the observed slopes of $j(NO_2)$ vs AOD are also larger than TUV-simulated slope at SSA of 0.95 and 0.85 when AOD is smaller than 0.8, and decreased rapidly with increasing AOD (panels c and d of Figure 5). The reason for this result is the same with that for $j(O^1D)$ as explained above.

Table 4 presents the slope, intercept and the determination coefficient (r^2) of linear fits of correlation between $j(NO_2)$ and AOD for each ozone column class at AOD smaller than 0.7. The slope of $j(NO_2)$ vs AOD also displays a significant dependence on SZA. The slope increases as SZA increases from 0 to 0.5 and then decreases as SZA increased from 0.5 to 1. At SZA of 60°±1 (cos (SZA)=0.5±0.015),

the respective slope of the linear regression indicates a reduction of $j(NO_2)$ by $3.2 \cdot 10^{-3}$ s^{-1} per AOD unit. This result is larger than the value for non-dust aerosols ($2.2 \cdot 10^{-3}$ s^{-1}) and close to the value for dust aerosols ($3.1 \cdot 10^{-3}$ s^{-1}) in the eastern Mediterranean reported by Gerasopoulos et al. (2012).

3.4 The parameterization relationship between photolysis frequencies, AOD, and SZA

As analyzed above, the photolysis frequencies ($j(O^1D)$ and $j(NO_2)$) strongly depended on AOD and cos(SZA) and could be fit into expression E5 using a quadratic polynomial form. Table 5 presents the fitting parametric equations and the corresponding coefficients of determination (R^2) at different O_3 column ranges. The coefficients of determination of the fitting equations are greater than 0.95 for $j(NO_2)$ and $j(O^1D)$, indicating that both of the photolysis frequencies strongly depended on AOD and cos(SZA) at a certain O_3 column, and the effect of other factors such as SSA and AE are integrated into the constant term in the parametric equation. Since the ozone column concentration has greater influence on $j(O^1D)$ than on $j(NO_2)$, the parameters of fitting equations for $j(NO_2)$ are similar, but the parameters of fitting equations for $j(O^1D)$ have a large fluctuation at different O_3 column ranges (especially a_1 and a_2). The parametric equations can be used to quantitatively evaluate the effect of AOD on photolysis frequencies in Beijing. According to the parametric equations,

aerosols lead to a decrease in j(NO_2) by 24.2% and 30.4% and a decrease in j(O^1D) by 27.3% and 32.6% in summer and winter, respectively, compared to an aerosol-free atmosphere. The decreasing ratio of the photolysis frequencies in winter is higher than in summer due to the higher SZA and lower SSA in winter.

The effect of aerosols on photolysis frequencies in Beijing is compared with other studies. Real and Sartelet (2011) reported a reduction in j(NO_2) and j(O^1D) of 13%-14% due to aerosols by using the radiative transfer code Fast-J during summer 2001 over European regions. Flynn et al (2010) reported that aerosols reduced j(NO_2) by 3% in Huston during 2006 by using TUV model. Gerasopoulos et al (2012) reported that aerosols reduced j(NO_2) and j(O^1D) by 5%-15% with 5-yr mean AOD at 380nm equal to 0.27. All of these results are lower than the reduction ratio of this study mainly due to higher aerosol level in Beijing (4-yr mean AOD equal to 0.76± 0.75). Hodzic et al. (2007) simulated a 15–30% j(NO_2) photolysis reduction during the 2003 European summer heatwave in the case of absorbing biomass burning aerosols with AOD at 550 nm equal to 0.7-0.8 and SSA at 532 nm equal to 0.83-0.87. The result of this study is comparable with the reduction ratio of this study possibly due to the equivalent levels of AOD and SSA. In addition, Péré et al (2015) simulated a higher reduction (20–50%) in j(NO_2) and j(O^1D) along the transport of the aerosol plume during the 2010 Russian summer wildfires episode. The higher reduction is due to the higher level of AOD (peak value of AOD at 400nm reached 2-4), even though SSA is very high (0.97).

$$j = a_1 + a_2 AOD + a_3 cos(SZA) + a_4 (AOD)^2 + a_5 AOD cos(SZA) + a_6 (cos(SZA))^2 \quad \text{...E5}$$

The above established parametric relationship of $PM_{2.5}$-AOD and $j(NO_2)$-AOD-SZA gives us a chance to estimate the effect of $PM_{2.5}$ on photolysis frequencies due to aerosol light extinction.

3.5 The influence of AOD on ozone production

In order to explain the effect of aerosol light extinction on ozone production, we used the data from the field observation campaign undertaken in August 2012. Ozone production depends on its precursors (NOx and VOCs), meteorological factors, and solar radiation. Solar radiation is the driving force for tropospheric photochemical reactions, in which $j(O^1D)$ and $j(NO_2)$ are both important for ozone production. On the one hand, the increase in $j(NO_2)$ promotes the photolysis of NO_2, thereby accelerating the formation of ozone. On the other hand, the increase in $j(O^1D)$ accelerates the photolysis of ozone. In addition, the increase in the photolysis frequencies will accelerate the photolysis of OVOC (especially formaldehyde and acetaldehyde), HONO, and H_2O_2, resulting in increases in OH and HO_2, which will promote the reaction between OH and VOCs and thus produce more RO_2. As a result, more ozone is produced by increasing the reaction rate between RO_2 (or HO_2) and NO. However, the increase in OH and HO_2 also consumes ozone and NO_2, which contributes to the increase in $D(O_3)$. In brief, the overall effect of changes in

450 photolysis frequencies on sources and sinks of ozone determines the change in the net
451 ozone production rate.

452 Ozone production (HO_2 + NO, RO_2 + NO), ozone loss (O^1D + H_2O, HO_2 + O_3,
453 O_3 + OH, NO_2 + OH, and O_3 + alkenes), and net ozone production rate during August
454 2012 were calculated by using the box model. We used the observed photolysis
455 frequencies (i.e. j_obs) and the calculated photolysis frequencies by parametric
456 equation under the condition of AOD equal to 0 (i.e. j_AOD=0), were used to
457 constrain the box model. The difference of simulated results in the two scenarios can
458 be attributed to the effect of aerosol light extinction. As a result, the presence of
459 aerosols causes a decrease in both ozone production rate and loss rate, as is shown in
460 Figure 8. Since the decreasing amplitude of the ozone production rate is far larger
461 than that of the ozone loss rate, the net production rate of ozone is reduced by 25%.
462 This reduction is comparable with the results of the study in Mexico City, where
463 aerosols caused a 20% reduction in the ozone concentrations (Castro et al., 2001).
464 Studies in Houston and Crete have shown that aerosols cause ozone production rates
465 to decrease by about 4% and 12%, respectively, which are lower than that found in
466 this study (Flynn et al., 2010; Gerasopoulos et al., 2012).

467 The ratio of the observed photolysis frequencies to the photolysis frequencies at
468 AOD equal to 0 is defined as JIF (Flynn et al., 2010). A JIF of less than 1 indicates
469 that the aerosols cause a decrease in the photolysis frequencies. Figure 9 shows the
470 relation between $P(O_3)_{j\_obs}/P(O_3)_{j\_AOD=0}$ (or $D(O_3)_{j\_obs}/D(O_3)_{j\_AOD=0}$) and JIF. The
471 majority of JIF values were less than 1, with an average of 0.72, indicating that

aerosols greatly attenuated photolysis frequencies due to high levels of AOD (average of 1.07) and low levels of SSA (average of 0.84) during the observation period. $P(O_3)_{j\_obs}/P(O_3)_{j\_AOD=0}$ and $D(O_3)_{j\_obs}/D(O_3)_{j\_AOD=0}$ are both linearly positively correlated with JIF and the scatters are mostly above the 1:1 line. As can be seen from the figure 9, a 30% reduction in photolysis frequencies (JIF = 0.7) due to the presence of aerosols results in a decrease in ozone production rate and loss rate by about 26% and 15%, respectively. The decreasing amplitude in the ozone production rate is greater than the decrease in the ozone loss rate because the corresponding processes of ozone production are all light-driven, but the corresponding processes of ozone loss are not all light-driven because the reaction of O_3 with alkenes does not depend on solar radiation. According to the simulated results, the reaction of ozone with alkenes during this campaign accounts for 17% of total ozone loss.

The diurnal profile of the mean ozone production and loss rate is shown in Figure 10. $P(O_3)$ peak midday in the 12:00-14:00 local hours at 31 ppb/h without aerosol impact and 23 ppb/h with aerosol impact. The maximum $D(O_3)$ also occurrs between 12:00 and 14:00 at 4.2 ppb/h without aerosol impact and 3.5 ppb/h with aerosol impact. There is little difference between aerosol-impact and aerosol-free $P(O_3)$ (or $D(O_3)$) in the hours of 6:00-11:00, but the difference in the afternoon (12:00-18:00) is large, indicating that the reduction effect of aerosol on ozone production mainly occurs during the afternoon.

The above analysis focuses on the effect of aerosol on the ozone production due to aerosol light extinction. However, it does not consider the close relationship

494 between aerosol and ozone's gaseous precursors in the actual atmosphere. To explain
495 this problem, we chose two adjacent days (small SZA effect) with obviously different
496 AOD levels: a clean day (A day: August 21, 2012; AOD = 0.21, $PM_{2.5}$=21.6 μg m^{-3})
497 and a day with high aerosol pollution (B day; August 26, 2012; AOD = 3.2,
498 $PM_{2.5}$=125.0 μg m^{-3}) (Table 7). The difference in AOD between the two days can be
499 taken to represent the maximum daytime gap of AOD for this month. The ozone
500 column concentrations for these two days were 302 DU and 301 DU, respectively, of
501 which the effect on $j(O^1D)$ is negligible. Under these conditions, the $j(O^1D)$ value at
502 noon time decreases from 3.23×10^5 s^{-1} on A day to 1.29×10^5 s^{-1} on B day (i.e., a 60%
503 reduction) and the $j(NO_2)$ value at noon time decreases from 8.26×10^{-3} s^{-1} on A day
504 to $4.19 \times 10^{-3} s^{-1}$ on B day (i.e., a 49.2% reduction). As shown in Table 7, B day has
505 higher AOD and higher concentrations of gaseous pollutants. The concentrations of
506 CO, NO_2, HCHO and the OH reactivity of VOCs in B day are much higher than in A
507 day, with the ratio of 3.6, 2.3, and 2.0, respectively. The simultaneous increases of
508 gaseous pollutants and AOD are due to the fact that gaseous pollutants (NOx, SO_2,
509 and VOCs) emitted by major pollution sources in Beijing, including traffic and
510 industry, have undergone the processes of gas-phase oxidation and nucleation to
511 generate secondary particulate matter that contributes to aerosol light extinction.
512 Previous studies have reported that secondary particulate matter has accounted for
513 more than 60% of total particulate matter during severe smog pollution in Beijing
514 summers (Han et al., 2015a; Guo et al., 2014). In addition, several studies have shown
515 that secondary components in particulate matter (especially secondary organics and

ammonium sulfate) have dominated the aerosol light extinction (Han et al., 2014; Han et al., 2017; Wang et al., 2015). Observations made in Beijing during the summer of 2006 showed that ammonium sulfate and ammonium nitrate contributed 44.6% and 22.3%, respectively, to the total extinction coefficient during a severe period of smog (Han et al., 2014); in the summer of 2014 in Beijing, ammonium sulfate, secondary organic aerosols, and ammonium nitrate contributed 30%, 22%, and 18%, respectively, to the total extinction coefficient (Han et al., 2017).

As shown in Figure 11, the simulation results indicate that the net $P(O_3)$ of B day is 36.2% higher than that of A day due to higher concentrations of ozone precursors on B day. This result is consistent with the observed ozone concentrations, of which the observed ozone concentration in B day is 2.2 times higher than that of A day. If we adjust the photolysis frequencies level of B day to the level of A day, the net $P(O_3)$ increases by 70.0%, which indicates that the high level of particulate matter in B day greatly inhibits ozone production. This result means that the system is under negative feedback, thus keeping O_3 at a relatively stable level. Table 8 summarizes the average levels of gaseous pollutants and photolysis frequencies for AOD less than 1 and greater than 1, as measured during August 2012. It shows that, the concentrations of ozone's precursors are higher and the photolysis frequencies are lower at high AOD levels (AOD > 1) than those at low AOD level (AOD < 1). This result means that the negative feedback mechanism is prevalent throughout the whole campaign period. Therefore, the prevention and control measures of air pollution in Beijing need to incorporate this coupling mechanism between particulate matter and ozone to achieve

effective control of these two main pollutants.

4. Conclusion

Photolysis reactions are important driving forces for tropospheric photochemical oxidation processes and ozone production. In this study, we explored in detail the effects of aerosols on photolysis frequencies and ozone production in Beijing, based on a long observation period of 4 years. We have found that:

(1) There is a strong correlation between $PM_{2.5}$ and AOD, and the slope in summer is smaller significantly than in winter, which indicates that aerosols in summer have a more efficient extinction capacity than in winter.

(2) As AOD increased, the extinction effect of aerosol on photolysis frequencies was decreased; this result was related to a higher proportion of scattering aerosols under high AOD conditions than under low AOD conditions. The slope of the correlation between photolysis frequencies and AOD indicates that the aerosols in urban Beijing have a stronger extinction on actinic flux than absorptive dust aerosols in the Mediterranean.

(3) The influence of AOD on photolysis frequencies was evaluated quantitatively by establishing parametric equations. According to the parametric equation, aerosols lead to a decrease in $j(NO_2)$ by 24.2% and 30.4% for summer and winter, respectively, and the corresponding decrease in $j(O^1D)$ by 27.3% and 32.6% respectively, compared to an aerosol-free atmosphere.

(4) In order to evaluate the effects of aerosols on ozone production rate, we carried out an observation campaign in August 2014. The results show that aerosols reduced the net ozone production rate by 25% by reducing the photolysis frequencies. High concentrations of ozone gaseous precursors were often accompanied by high concentrations of particulate matter, which, to a large extent, inhibited excessive levels of ozone generation and reflected the negative feedback effect of the atmospheric system. Therefore, the influence of aerosol on photolysis frequencies and thus on the rate of oxidation of VOCs and NOx to ozone and secondary aerosol is important for determining the atmospheric effects of controlling the precursor emissions of these two important air pollutants (aerosols and ozone).

Author contribution

Author	Contribution
Wenjie Wang	acquisition of data; analysis and interpretation of data; drafting the article and revising it critically
Min Shao	substantial contributions to conception and design; revising the article critically
Min Hu	collection of data
Limin Zeng	collection of data
Yusheng Wu	collection of data

ACKNOWLEDGEMENTS

This work was supported by the Major Program of the National Natural Science Foundation of China [Grant number 91644222]. We thank Hongbin Chen and Philippe Goloub for data management of AOD and other aerosol optical properties on AERONET.

Reference

Barnarda, J. C., Chapmana E G., Fasta, J. D., Schmelzera, J. R., Slusserb, J. R., Shetterc, R. E.: An evaluation of the FAST-Jphotolysis algorithm for predicting nitrogen dioxide photolysis rates under clear and cloudy sky conditions, ATMOSPHERIC ENVIRONMENT, 38, 3393-3403, 10.1016/j.atmosenv.2004.03.034, 2004.

Bohn, B., Corlett, G. K., Gillmann, M., Sanghavi, S., Stange, G., Tensing, E., Vrekoussis, M., Bloss, W. J., Clapp, L. J., Kortner, M., Dorn, H. P., Monks, P. S., Platt, U., Plass-Dulmer, C., Mihalopoulos, N., Heard, D. E., Clemitshaw, K. C ., Meixner, F. X., Prevot, A. S. H., Schmitt, R.: Photolysis frequency measurement techniques: Results of a comparison within the ACCENT project, ATMOSPHERIC CHEMISTRY AND PHYSICS, 8, 5373–5391, doi:10.5194/acp-8-5373-2008, 2008.

Casasanta, G., di Sarra, A., Meloni, D., Monteleone, F., Pace, G., Piacentino, S., Sferlazzo, D.: Large aerosol effects on ozone photolysis in the Mediterranean, ATMOSPHERIC ENVIRONMENT, 45, 3937-3943, 10.1016/j.atmosenv.2011.04.065, 2011.

Castro, T., Madronich, S., Rivale, S., Muhlia, A., Mar, B.: The influence of aerosols on photochemical smog in Mexico City, ATMOSPHERIC ENVIRONMENT, 35, 1765-1772, 10.1016/S1352-2310(00)00449-0, 2001.

Chang, D, Song, Y, Liu, B.: Visibility trends in six megacities in China 1973–2007, ATMOSPHERIC RESEARCH, 94, 161-167, 10.1016/j.atmosres.2009.05.006, 2009.

Che, H., Zhang, X., Li, Y., Zhou, Z., Qu, J. J., Hao, X.: Haze trends over the capital cities of 31 provinces in China, 1981–2005, THEORETICAL AND APPLIED CLIMATOLOGY, 97, 235-242, 10.1007/s00704-008-0059-8, 2009.

de Miranda, R., Andrade, M. F., Fattori, A. P.: Preliminary studies of the effect of aerosols on nitrogen dioxide photolysis rates in the city of Sao Paulo, Brazil.

625 ATMOSPHERIC RESEARCH, 75, 135–148, 10.1016/j.atmosres.2004.12.004,
626 2005.
627 Dickerson, R. R., Kondragunta, S., Stenchikov, G., Civerolo, K. L., Doddridge, B. G.,
628 Holben, N.: The impact of aerosols on solar ultraviolet radiation and
629 photochemical smog, Science, 278, 827–830, 10.1126/science.278.5339.827,
630 1997.
631 Ehhalt, D. H., Rohrer, F.: Dependence of the OH concentration on solar UV,
632 JOURNAL OF GEOPHYSICAL RESEARCH-ATMOSPHERES, 105**,**
633 3565-3571, 10.1029/1999JD901070, 2000.
634 Finlayson-Pitts, B. J., Pitts, J. N.: Chemistry of the Upper and Lower Atmosphere.
635 Academic Press, New York, 2000.
636 Flynn, J., Lefer, B., Rappenglück, B., Leuchner, M., Perna, R., Dibb, J., Ziemba, L.,
637 Anderson, C., Stutz, J., Brune, W., Ren, X. R.: Impact of clouds and aerosols on
638 ozone production in Southeast Texas. ATMOSPHERIC ENVIRONMENT, 44,
639 4126–4133, 10.1016/j.atmosenv.2009.09.005, 2010.
640 Fotiadi, A., Hatzianastassiou, N., Drakakis, E., Matsoukas, C., Pavlakis, K. G.,
641 Hatzidimitriou, D., Gerasopoulos, E., Mihalopoulos, N., Vardavas, I.: Aerosol
642 physical and optical properties in the eastern Mediterranean Basin, Crete, from
643 Aerosol Robotic Network data, ATMOSPHERIC CHEMISTRY AND PHYSICS,
644 6, 5399–5413, 10.5194/acp-6-5399-2006, 2006
645 Gao W, Tie X X, Xu J M, Huang R J, Mao X Q, Zhou G Q, Luyu Chang. Long-term
646 trend of O3 in a mega City (Shanghai), China: Characteristics, causes, and
647 interactions with precursors. SCIENCE OF THE TOTAL ENVIRONMENT, 603,
648 425–433, 10.1016/j.scitotenv.2017.06.099, 2017.
649 Garland, R.; O. Schmid, A.; Nowak, P.; Achtert, A.; Wiedensohler, S.; Gunthe, N.;
650 Takegawa, K.; Kita, Y.; Kondo, and M. Hu (2009), Aerosol optical properties
651 observed during Campaign of Air Quality Research in Beijing 2006
652 (CAREBeijing-2006): Characteristic differences between the inflow and outflow

of Beijing city air, JOURNAL OF GEOPHYSICAL RESEARCH-ATMOSPHERES, 114, D00G04, 10.1029/2008JD010780, 2009.

Gerasopoulos, E., Kazadzis, S., Vrekoussis, M., Kouvarakis, G., Liakakou, E., Kouremeti, N., Giannadaki, D., Kanakidou, M., Bohn, B., Mihalopoulos, N.: Factors affecting O_3 and NO_2 photolysis frequencies measured in the eastern Mediterranean during the five-year period 2002–2006, JOURNAL OF GEOPHYSICAL RESEARCH-ATMOSPHERES, 117, D22305, 10.1029/2012JD017622, 2012.

Goliff, W. S., Stockwell, W. R., Lawson, C. V.: The regional atmospheric chemistry mechanism, version 2, ATMOSPHERIC ENVIRONMENT, 68: 174–185, 10.1016/j.atmosenv.2012.11.038, 2013.

Guo, S., Hu M, Zamora, M. L., Peng, J. F., Shang, D. J., Zheng, J., Du, Z. F., Wu, Z. J., Shao, M., Zeng, L. M., Molina, M. J., Zhang, R. Y.: Elucidating severe urban haze formation in China, PROCEEDINGS OF THE NATIONAL ACADEMY OF SCIENCES OF THE UNITED STATES OF AMERICA, 111: 17373–17378, 10.1073/pnas.1419604111, 2014.

Han, T. T., Liu, X. G., Zhang, Y. H., Qu, Y.,Gu, J. W., Ma, Q., Lu, K. D., Tian, H. Z,, Chen, J., Zeng, L. M.: Characteristics of aerosol optical properties and their chemical apportionments during CAREBeijing 2006, AEROSOL AND AIR QUALITY RESEARCH,14: 1431-1442, 10.4209/aaqr.2013.06.0203, 2014.

Han, T. T., Xu, W. Q., Chen, C., Liu, X. G., Wang, Q. Q., Li, J., Zhao, X. J., Du, W., Wang, Z. F., Sun, Y. L.: Chemical apportionment of aerosol optical properties during the Asia-Pacific Economic Cooperation summit in Beijing, China, JOURNAL OF GEOPHYSICAL RESEARCH-ATMOSPHERES, 120, 10.1002/2015JD023918, 2015b.

Han, T. T., Xu, W. Q., Li, J., Freedman, A., Zhao, J., Wang, Q. Q., Chen, C., Zhang, Y. J., Wang, Z. F., Fu, P. Q.: Aerosol optical properties measurements by a CAPS single scattering albedo monitor: Comparisons between summer and winter in Beijing, China, JOURNAL OF GEOPHYSICAL RESEARCH-ATMOSPHERES,

122, 2513-2526, 10.1002/2016JD025762, 2017.

Han, T., Liu, X., Zhang, Y., Qu, Y., Zeng, L., Hu, M., Zhu, T.: Role of secondary aerosols in haze formation in summer in the Megacity Beijing, JOURNAL OF ENVIRONMENTAL SCIENCES, 31, 51-60, 10.1016/j.jes.2014.08.026, 2015a.

He, S., Carmichael, G. R.: Sensitivity of photolysis rates and ozone production in the troposphere to aerosol properties, JOURNAL OF GEOPHYSICAL RESEARCH-ATMOSPHERES, 104, 26307–26324, 10.1029/1999JD900789, 1999.

Hendrick, F; Muller, JF; Clemer, K; Wang, P; De Maziere, M; Fayt, C; Gielen, C; Hermans, C; Ma, JZ; Pinardi, G ; Stavrakou, T; Vlemmix, T; Van Roozendael, M., Four years of ground-based MAX-DOAS observations of HONO and NO_2 in the Beijing area. ATMOSPHERIC CHEMISTRY AND PHYSICS, 14(2), 765-781, 2014.

Hodzic, A., Madronich, S., Bohn, B., Massie, S., Menut, L., and Wiedinmyer, C.: Wildfire particulate matter in Europe during summer 2003: meso-scale modeling of smoke emissions, trans-port and radiative effects, ATMOSPHERIC CHEMISTRY AND PHYSICS, 7, 4043–4064, 10.5194/acp-7-4043-2007, 2007.

Hofzumahaus, A., Kraus, A., Muller, M.: Solar actinic flux spectroradiometry: A technique for measuring photolysis frequencies in the atmosphere, APPLIED OPTICS, 38, 4443–4460, 10.1364/AO.38.004443, 1999.

Hofzumahaus, A., Lefer, B. L., Monks, P. S., Hall, S. R., Kylling, A., Mayer, B., Shetter, R. E., Junkermann, W., Bais, A., Calvert, J. G., Cantrell, C. A., Madronich, S., Edwards, G. D., Kraus, A.: Photolysis frequency of O_3 to $O(^1D)$: Measurements and modeling during the International Photolysis Frequency Measurement and Modeling Intercomparison (IPMMI), JOURNAL OF GEOPHYSICAL RESEARCH-ATMOSPHERES, 109 (D8), D08S90, 10.1029/2003JD004333, 2004.

Jacobson, M, Z.: Studying the effects of aerosols on vertical photolysis rate coefficient and temperature profiles over an urban airshed, JOURNAL OF

711 GEOPHYSICAL RESEARCH-ATMOSPHERES, 103, 10593–10604,
712 10.1029/98JD00287, 1998.
713 Lefer, B. L., Shetter, R. E., Hall, S. R.: Impact of clouds and aerosols on photolysis
714 frequencies and photochemistry during TRACE-P: 1. Analysis using radiative
715 transfer and photochemical box models, JOURNAL OF GEOPHYSICAL
716 RESEARCH-ATMOSPHERES, 108, 8821-8835, 10.1029/2002JD003171, 2003.
717 Li C C, Mao J T, Liu Q H. Using MODIS to study the distribution and seasonal
718 variation of aerosol optical thickness in eastern China. Science Bulletin (China),
719 48: 2094-2100. 2003.
720 Li, J., Wang, Z. F., Wang, X., Yamaji, K., Takigawa, M., Kanaya, Y., Pochanart, P.,
721 Liu, Y., Irie, H., Hu, B., Tanimoto, H., Akimoto, H.: Impacts of aerosols on
722 summertime tropospheric photolysis frequencies and photochemistry over
723 Central Eastern China, ATMOSPHERIC ENVIRONMENT, 45: 1817-1829,
724 10.1016/j.atmosenv.2011.01.016, 2011.

725 Liao, H., Yung, Y. L., and Seinfeld, J. H.: Effects of aerosols on tropospheric
726 photolysis rates in clear and cloudy atmospheres, JOURNAL OF
727 GEOPHYSICAL RESEARCH, 104(D19), 23697–23707, 1999.

728 Liu, Q.Y., Ma, T. M., Olson, M. R., Liu, Y. J., Zhang, T. T., Wu, Y., Schauer, J. J.:
729 Temporal variations of black carbon during haze and non-haze days in Beijing,
730 SCIENTIFIC REPORTS, 6, 33331, 10.1038/srep33331, 2016.
731 Lou, S. J; Liao, H; Zhu, B. Impacts of aerosols on surface-layer ozone concentrations
732 in China through heterogeneous reactions and changes in photolysis rates.
733 ATMOSPHERIC ENVIRONMENT, 85:123-138,
734 0.1016/j.atmosenv.2013.12.004, 2014.
735 Lu, K. D., Rohrer, F., Holland, F., Fuchs, H., Bohn, B., Brauers, T., Chang, C. C.,
736 Häseler, R., Hu, M., Kita, K., Kondo, Y., Li, X., Lou, S. R., Nehr, S., Shao, M.,
737 Zeng, L. M., Wahner, A., Zhang, Y. H., Hofzumahaus, A.: Observation and
738 modelling of OH and HO_2 concentrations in the Pearl River Delta 2006: a

missing OH source in a VOC rich atmosphere, ATMOSPHERIC CHEMISTRY AND PHYSICS, 12: 1541-1569, 10.5194/acp-12-1541-2012, 2012

Ma, X. Y., Wang, J. Y., Yu, F. Q., Jia, H. L., Hu, Y. N.: Can MODIS AOD be employed to derive PM2.5 in Beijing-Tianjin-Hebei over China? ATMOSPHERIC RESEARCH, 181, 250-256, 10.1016/j.atmosres.2016.06.018, 2016.

Ma, Z. W., Hu, X. F., Huang, L., Bi, J., Liu, Y.: Estimating Ground-Level $PM_{2.5}$ in China Using Satellite Remote Sensing. Environ Sci Technol, 48: 7436−7444.

Madronich, S, The Atmosphere and UV-B Radiation at Ground Level, Environmental UV Photobiology, doi: 0.1007/978-1-4899-2406-3_1. 1993,

Madronich, S., and S. Flocke, The role of solar radiation in atmospheric chemistry, in Environmental Photochemistry, edited by P. Boule, pp. 1-26, Springer-Verlag, New York, 1999.

Mailler, S., Menut, L., di Sarra, A. G., Becagli, S., Di Iorio, T., Bessagnet, B., Briant, R., Formenti, P., Doussin, J. F ., Gomez-Amo, J. L., Mallet, M., Rea, G., Siour, G., Sferlazzo, D. M., Traversi, R., Udisti, R., Turquety, S.: On the radiative impact of aerosols on photolysis rates: comparison of simulations and observations in the Lampedusa island during the ChArMEx/ADRIMED campaign, ATMOSPHERIC CHEMISTRY AND PHYSICS, 16(3):1219-1244, 10.5194/acp-16-1219-2016, 10.5194/acp-16-1219-2016, 2016.

Peeters, J., Nguyen, T. L., Vereecken, L.: HOX radical regeneration in the oxidation of isoprene. PHYSICAL CHEMISTRY CHEMICAL PHYSICS, 11: 5935-5939, 10.1039/b908511d, 2009.

Pere, J. C., Bessagnet, B., Pont, V., Mallet, M., Minvielle, F.: Influence of the aerosol solar extinction on photochemistry during the 2010 Russian wildfires episode, ATMOSPHERIC CHEMISTRY AND PHYSICS, 15**,** 10983-10998, 10.5194/acp-15-10983-2015, 2015.

Raga, G. B., Castro, T., Baumgardner, D.: The impact of megacity pollution on local

767 climate and implications for the regional environment: Mexico City,
768 ATMOSPHERIC ENVIRONMENT, 35, 1805-1811,
769 10.1016/S1352-2310(00)00275-2, 2001.

770 Real, E. and Sartelet, K.: Modeling of photolysis rates over Europe: impact on
771 chemical gaseous species and aerosols, ATMOSPHERIC CHEMISTRY AND
772 PHYSICS, 11, 1711–1727, 10.5194/acp-11-1711-2011, 2011.

773 Rohrer, F; Lu, K. D; Hofzumahaus, A; Bohn, B ; Brauers, T ; Chang, C. C ; Fuchs, H;
774 Haseler, R; Holland, F; Hu, M., Maximum efficiency in the
775 hydroxyl-radical-based self-cleansing of the troposphere, Nature Geoscience. 7,
776 559-563, 2014.

777 Shetter, R. E., Muller, M.: Photolysis frequency measurements using actinic flux
778 spectroradiometry during PEM-Tropics Mission: Instrumentation description and
779 some results, JOURNAL OF GEOPHYSICAL RESEARCH-ATMOSPHERES,
780 104, 5647-5661, 10.1029/98JD01381, 1999.

781 Shetter, R. E.: Photolysis frequency of NO2: measurement and modeling during the
782 International Photolysis Frequency Measurement and Modeling Intercomparison
783 (IPMMI), JOURNAL OF GEOPHYSICAL RESEARCH-ATMOSPHERES, 108,
784 8544, 10.1029/2002JD002932, 2003.

785 Stone, D; Whalley, L. K; Heard, D. E. Tropospheric OH and HO_2 radicals: field
786 measurements and model comparisons, Chem. Soc. Rev,41(19): 6348-6404,
787 10.1039/c2cs35140d, 2012.

788 Tang, Y., Carmichael, G. R., Kurata, G., Uno, I., Weber, R. J., Song, C. H., Guttikunda,
789 S. K., Woo, J. H., Streets, D. G., Wei, C., Clarke, A. D., Huebert, B., Anderson, T.
790 L.: Impacts of dust on regional tropospheric chemistry during the ACE-Asia
791 experiment: a model study with observations, JOURNAL OF GEOPHYSICAL
792 RESEARCH-ATMOSPHERES, 109, D19S21, 10.1029/2003JD003806, 2004.

793 Tian, P., Wang, G. F., Zhang, R. J., Wu, Y. F., Yan, P.: Impacts of aerosol chemical
794 compositions on optical properties in urban Beijing, China, PARTICUOLOGY,
795 18, 155-164, 10.1016/j.partic.2014.03.014, 2015.

796 Tie, X. X., Madronich, S., Walters, S., Edwards, D. P., Ginoux, P., Mahowald, N.,
797 Zhang, R. Y., Lou, C., Brasseur, G.: Assessment of the global impact of aerosols
798 on tropospheric oxidants. JOURNAL OF GEOPHYSICAL
799 RESEARCH-ATMOSPHERES, 110, D03204, 10.1029/2004JD005359, 2005.
800 van Donkelaar, A., Martin, R. V., Brauer, M., Kahn, R., Levy, R., Verduzco, C., and
801 Villeneuve, P. J.: Global Estimates of Ambient Fine Particulate Matter
802 Concentrations from Satellite-Based Aerosol Optical Depth: Development and
803 Application. Environmental Health Perspectives, 118, 847-855,
804 10.1289/ehp.0901623, 2010.
805 Verstraeten, W, W., Neu, J. L., Williams, J. E., Bowman, K. W., Worden, J. R.,
806 Boersma, K. F.: Rapid increases in tropospheric ozone production and export
807 from China. NATURE GEOSCIENCE, 8, 690-695, 10.1038/NGEO2493, 2015.
808 Volkamer R, Sheehy P, Molina L T, Molina M J.: Oxidative capacity of the Mexico
809 City atmosphere – Part 1: A radical source perspective, ATMOSPHERIC
810 CHEMISTRY AND PHYSICS, 10, 6969–6991, 10.5194/acp-10-6969-2010,
811 2010.
812 Wang, B.,Shao, M., Lu, S. H., Yuan, B., Zhao, Y., Wang, M., Zhang, S. Q., Wu, D.:
813 Variation of ambient non-methane hydrocarbons in Beijing city in summer 2008,
814 ATMOSPHERIC CHEMISTRY AND PHYSICS, 10, 5911–5923,
815 10.5194/acp-10-5911-2010, 2010.
816 Wang, Q., Sun, Y., Jiang, Q., Du, W., Sun, C., Fu, P., Wang, Z.: Chemical
817 composition of aerosol particles and light extinction apportionment before and
818 during the heating season in Beijing, China. JOURNAL OF GEOPHYSICAL
819 RESEARCH-ATMOSPHERES, 120: 12,708-12,722, 10.1002/2015JD023871,
820 2015.
821 Xin, J. Y; Gong, C. S; Liu, Z. R; Cong, Z. Y; Gao, W. K; Song, T; Pan, Y. P; Sun, Y;
822 Ji, D. S; Wang, L. L; Tang, G. Q; Wang, Y. S.: The observation-based
823 relationships between $PM_{2.5}$ and AOD over China, JOURNAL OF

GEOPHYSICAL RESEARCH-ATMOSPHERES, 121, 10701-10716, 10.1002/2015JD024655, 2016.

Xu, J., Ma, J. Z., Zhang, X. L., Xu, X. B., Xu, X. F., Lin, W. L., Wang, Y., Meng, W., and Ma, Z. Q.: Measurements of ozone and its precursors in Beijing during summertime: impact of urban plumes on ozone pollution in downwind rural areas, ATMOSPHERIC CHEMISTRY AND PHYSICS, 11, 12241–12252, 10.5194/acp-11-12241-2011, 2011.

Zhang, J. P., Zhu, T., Zhang, Q. H., Li, C. C., Shu, H. L., Ying, Y., Dai, Z. P., Wang, X., Liu, X. Y., Liang, A. M., Shen, H. X., and Yi, B. Q.: The impact of circulation patterns on regional transport pathways and air quality over Beijing and its surroundings, ATMOSPHERIC. CHEMISTRY AND PHYSICS, 12, 5031–5053, 10.5194/acp-12-5031-2012, 2012.

Zhang, L.; Shao, J.; Lu, X.; Zhao, Y.; Hu, Y.; Henze, D. K.; Liao, H.; Gong, S.; Zhang, Q.: Sources and Processes Affecting Fine Particulate Matter Pollution over North China: An Adjoint Analysis of the Beijing APEC Period. ENVIRONMENTAL SCIENCE & TECHNOLOGY, 50(16), 8731-8740, 10.1021/acs.est.6b03010, 2016.

Zhang, Q., Yuan, B., Shao, M., Wang, X., Lu, S., Lu, K., Wang, M., Chen, L., Chang, C. C., Liu, S. C.: Variations of ground-level O3 and its precursors in Beijing in summertime between 2005 and 2011, ATMOSPHERIC CHEMISTRY AND PHYSICS, 14, 6089-6101, 10.5194/acp-14-6089-2014, 2014.

Zhang, R., Jing, J., Tao, J., Hsu, S. C., Wang, G., Cao, J., Lee, C. S. L., Zhu, L., Chen, Z., Zhao, Y., Shen, Z.: Chemical characterization and source apportionment of $PM_{2.5}$ in Beijing: seasonal perspective, ATMOSPHERIC CHEMISTRY AND PHYSICS, 13, 7053-7074, 10.5194/acp-13-7053-2013, 2013.

Zheng, C. W., Zhao, C. F., Zhu, Y. N., Wang, Y., Shi, X. Q., Wu, X. L., Chen, T. M., Wu, F., Qiu, Y. M.: Analysis of influential factors for the relationship between $PM_{2.5}$ and AOD in Beijing, ATMOSPHERIC CHEMISTRY AND PHYSICS, 17, 13473-13489, 10.5194/acp-17-13473-2017, 2017.

Table 1. Instruments deployed in the field campaign undertaken in August 2012 and used for data analysis.

Parameters	Measurement technique	Time resolution	Detection limit	Accuracy
$j(O^1D)$ and $j(NO_2)$	Spectroradiometer	10 s	/	± 10%
O_3	UV photometry	60 s	0.5 ppbv	± 5%
NO	Chemiluminescence	60 s	60 pptv	± 20%
NO_2	Chemiluminescence	60 s	300 pptv	± 20%
CO	IR photometry	60 s	4 ppb	± 5%
SO_2	Pulsed UV fluorescence	60 s	0.1 ppbv	± 5%
HCHO	Hantzsch fluorimetry	60 s	25 pptv	± 5%
VOCs	GC-FID/MS	1 h	20-300 pptv	± 15~20%

Table 2. O_3 column concentration, temperature relative humidity and respective standard deviation for different seasons.

	O_3 column (Du)	Temperature (℃)	Relative humidity (%)
Spring	354.9±37.3	15.6±7.8	33.2±18.1
Summer	310.2±23.8	27.5±4.2	57.2±17.7
Autumn	303.8±22.8	15.5±7.4	46.4±20.6
Winter	347.2±28.2	0.53±4.24	30.4±17.6

Table 3. Slope, intercept and the square of correlation coefficient (r^2) of linear fits of correlation between $j(O^1D)$ and AOD for each ozone column class at AOD smaller than 0.7.

	SZA=30°			SZA=60°		
O_3 column (DU)	Slope ($10^{-6}s^{-1}$)	Intercept ($10^{-6}s^{-1}$)	r^2	Slope ($10^{-6}s^{-1}$)	Intercept ($10^{-6}s^{-1}$)	r^2
300-330	-6.24±1.52	25.7±0.8	0.34	-4.21±0.43	7.67±0.33	0.41
330-360	-6.50±1.43	23.2±0.6	0.40	-5.01±0.34	7.15±0.21	0.52
360-390	-9.45±1.64	20.9±0.9	0.52	-6.93±0.62	7.59±0.34	0.66

Table 4. Slope, intercept and the square of correlation coefficient (r^2) of linear fits of correlation between $j(NO_2)$ and AOD for each ozone column class at AOD smaller than 0.7.

cos(SZA)	Slope (10^{-3} s^{-1})	Intercept (10^{-3} s^{-1})	r^2
0-0.2	-1.28±0.07	1.54±0.04	0.52
0.2-0.4	-2.44±0.10	3.40±0.04	0.41
0.4-0.6	-3.20±0.09	5.49±0.04	0.49
0.6-0.8	-2.08±0.09	7.20±0.05	0.38
0.8-1.0	-1.77±0.12	8.12±0.05	0.26

Table 5. The fitting parameters a_1-a_6 and determination coefficients of E5 for $j(NO_2)$.

O_3 column (DU)	a_1	a_2	a_3 $\times10^{-3}$	a_4	a_5	a_6	r^2
270-300	-0.20 ± 0.09	-2.1 ± 0.1	13.1 ± 0.4	0.27± 0.02	0.19 ± 0.09	-3.5± 0.3	0.96
300-330	-0.48 ± 0.07	-1.9 ± 0.1	13.3 ± 0.3	0.19 ± 0.01	0.34±0.08	-3.9±0.3	0.96
330-360	-0.22 ± 0.08	-2.2 ± 0.1	11.8 ± 0.3	0.42 ± 0.03	0.23±0.03	-2.6±0.2	0.96
360-400	-0.21± 0.10	-2.0± 0.1	12.6 ± 0.2	0.18±0.02	0.39±0.03	-4.0±0.3	0.95

Table 6. The fitting parameters a_1-a_6 and determination coefficients of E5 for $j(O^1D)$.

O_3 column (Du)	a_1	a_2	a_3 $\times10^{-6}$	a_4	a_5	a_6	r^2
270-300	0.88 ± 0.30	-0.10± 0.21	-5.1 ± 0.5	0.93± 0.06	-8.6 ± 0.4	43.9± 0.8	0.96
300-330	0.58 ± 0.07	0.13 ± 0.17	-3.8± 0.8	0.68 ± 0.04	-7.1 ± 0.2	37.1 ± 0.8	0.96
330-360	2.2 ± 0.20	-0.65 ± 0.19	-9.8± 0.9	1.01 ± 0.07	-6.3 ± 0.3	38.1 ± 0.6	0.97
360-400	2.0 ± 0.10	-0.72 ± 0.40	-7.0 ± 0.5	0.76 ± 0.08	-6.2± 0.7	33.0 ± 0.8	0.95

Table 7. Mean and standard deviation of observed data during daytime (6:00–18:00) for A day and B day.

Observed data	A day: August 21, 2012	B day: August 26, 2012
AOD	0.21 ± 0.05	3.2 ± 0.4
$PM_{2.5}$ ($\mu g\ m^{-3}$)	21.6 ± 9.0	125.0 ± 15.7
O_3 column (Du)	302 ± 3.0	301± 3.0
Temperature(°C)	27.6 ± 3.3	27.6 ± 3.2
Relative humidity (%)	47.6 ± 10.1	54.5 ± 11.8
$j(O^1D)(s^{-1})$	$1.57\times 0^{-5} \pm 1.24\times10^{-5}$	$6.87\times10^{-6} \pm 5.2\times10^{-6}$
$j(NO_2)(s^{-1})$	$5.37\times10^{-3} \pm 2.88\times10^{-3}$	$2.87\times10^{-3} \pm 1.65\times10^{-3}$
O_3 (ppb)	39.7 ± 16.56	86.8 ± 52.82
NO_2 (ppb)	10.7 ± 5.0	24.9 ± 9.6
CO (ppm)	0.24 ± 0.05	0.85 ± 0.14
VOC reactivity (s^{-1})	3.0 ± 0.7	6.4 ± 1.7
HCHO (ppb)	2.7± 1.1	7.4± 1.9

Table 8. Monthly mean and standard deviation of observed data during daytime (6:00–18:00) under the condition of AOD less than 1 and larger than 1 in August 2012

Observed data	AOD<1	AOD>1
AOD	0.43 ± 0.24	2.0 ± 0.8
$PM_{2.5}$ ($\mu g\ m^{-3}$)	26.4 ± 12.4	76.9 ± 47.1
O_3 column (Du)	303 ± 4.0	302 ± 5.0
Temperature(°C)	29.6 ± 4.3	29.2 ± 4.1
Relative humidity (%)	42.1 ± 15.8	57.0 ± 12.8
$j(O^1D)(s^{-1})$	$1.62\times10^{-5} \pm 1.05\times10^{-5}$	$1.03\times10^{-5} \pm 0.67\times10^{-5}$
$j(NO_2)(s^{-1})$	$5.64\times10^{-3} \pm 2.42\times10^{-3}$	$3.80\times10^{-3} \pm 1.66\times10^{-3}$
O_3 (ppb)	52.4 ± 33.8	67.9 ± 45.7
NO_2 (ppb)	16.4 ± 7.8	24.4 ± 8.9
CO (ppm)	0.47 ± 0.20	0.95 ± 0.47
VOC reactivity (s^{-1})	4.3 ± 1.7	6.2 ± 2.2
HCHO (ppb)	4.0 ± 1.4	6.5± 1.9

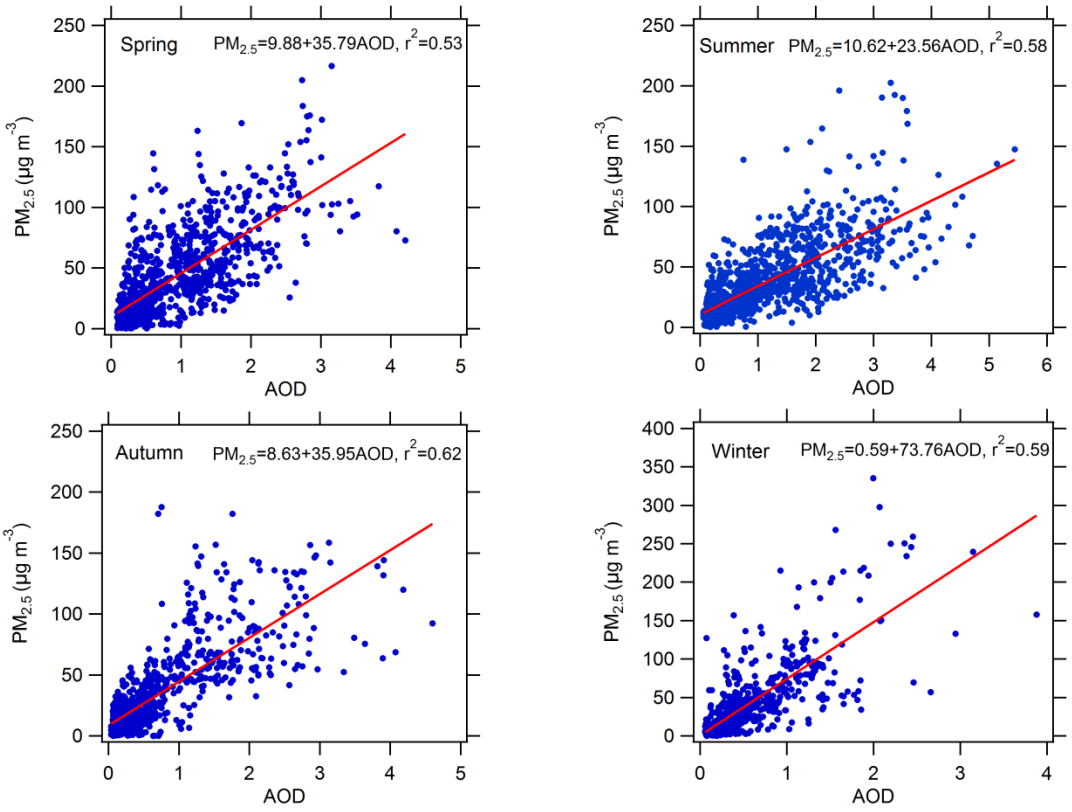

Figure 1. Scatter plots between AOD at 380nm and $PM_{2.5}$ in four different seasons. The slope, intercept and determination coefficient (r^2) were calculated.

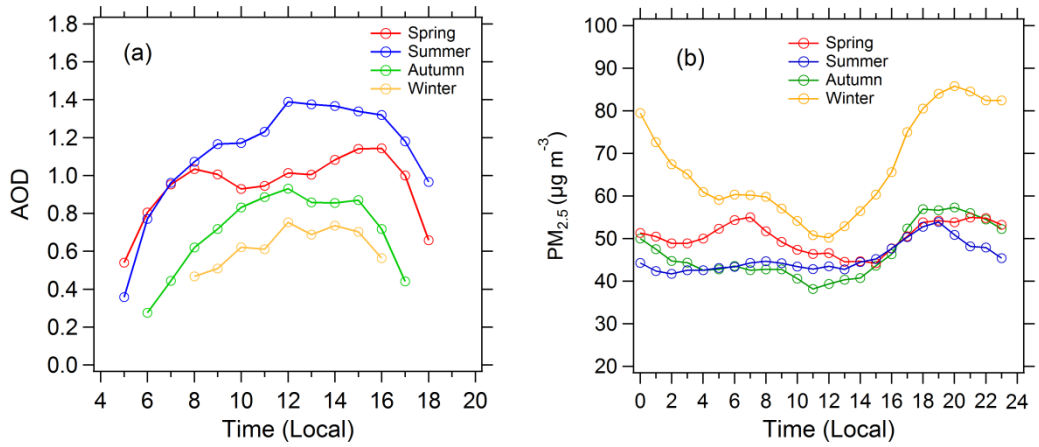

Figure 2. Diurnal cycles of (a) AOD and (b) $PM_{2.5}$ in the four seasons.

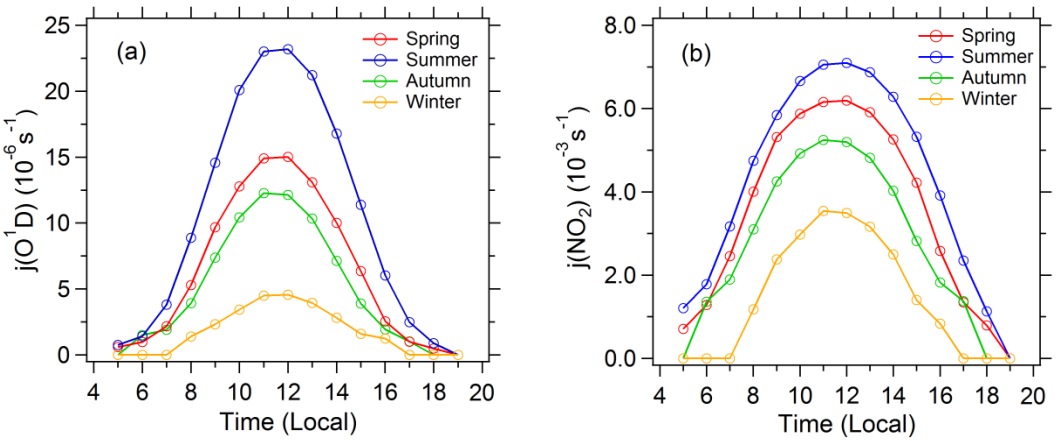

Figure 3. Diurnal cycles of (a) $j(O^1D)$ and (b) $j(NO_2)$ in the four seasons under cloudless conditions.

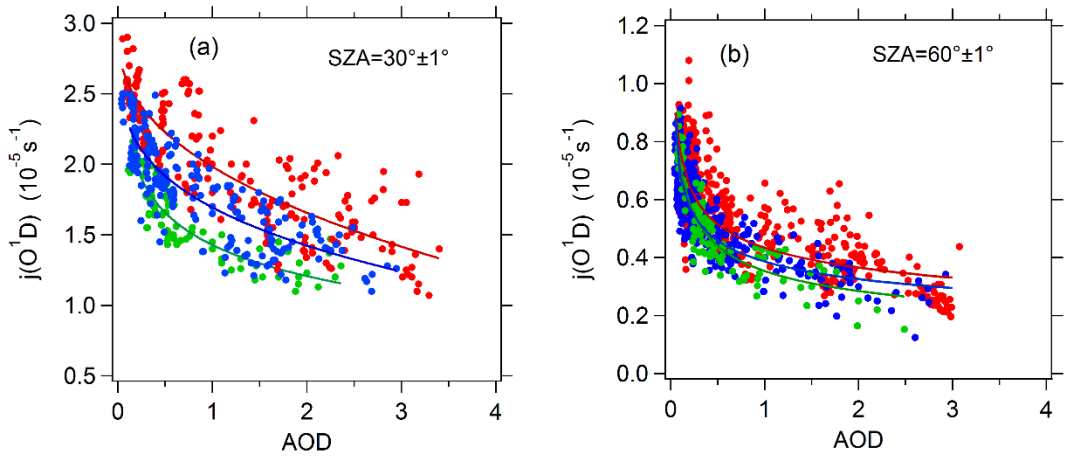

Figure 4. Dependence of $j(O^1D)$ on AOD at SZA of (a) 30° and (b) 60° and at different classes of ozone column concentration: 300-330 DU (red), 330-360 DU (blue), and 360-390 DU (green).

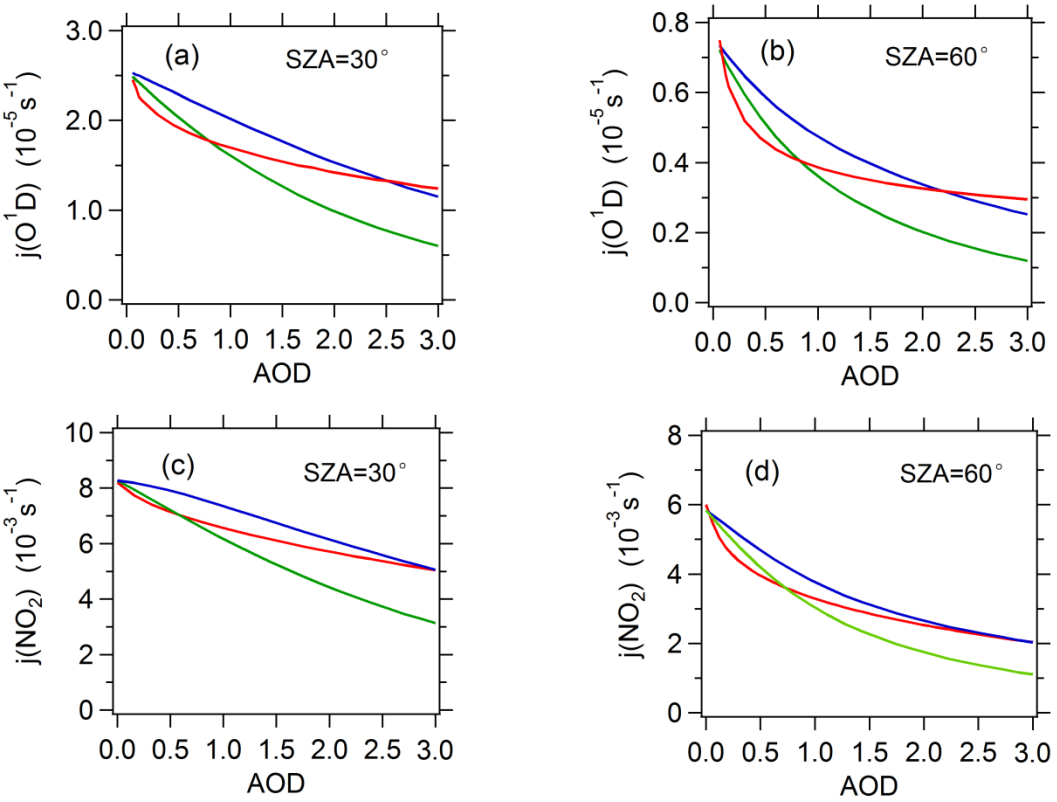

Figure 5. The relationship between observed or TUV-simulated photolysis frequencies and AOD at SZA of 30° and 60°. The red line represents observed average photolysis frequencies; the blue line and green line represents TUV-simulated photolysis frequencies at SSA of 0.95 and 0.85 respectively.

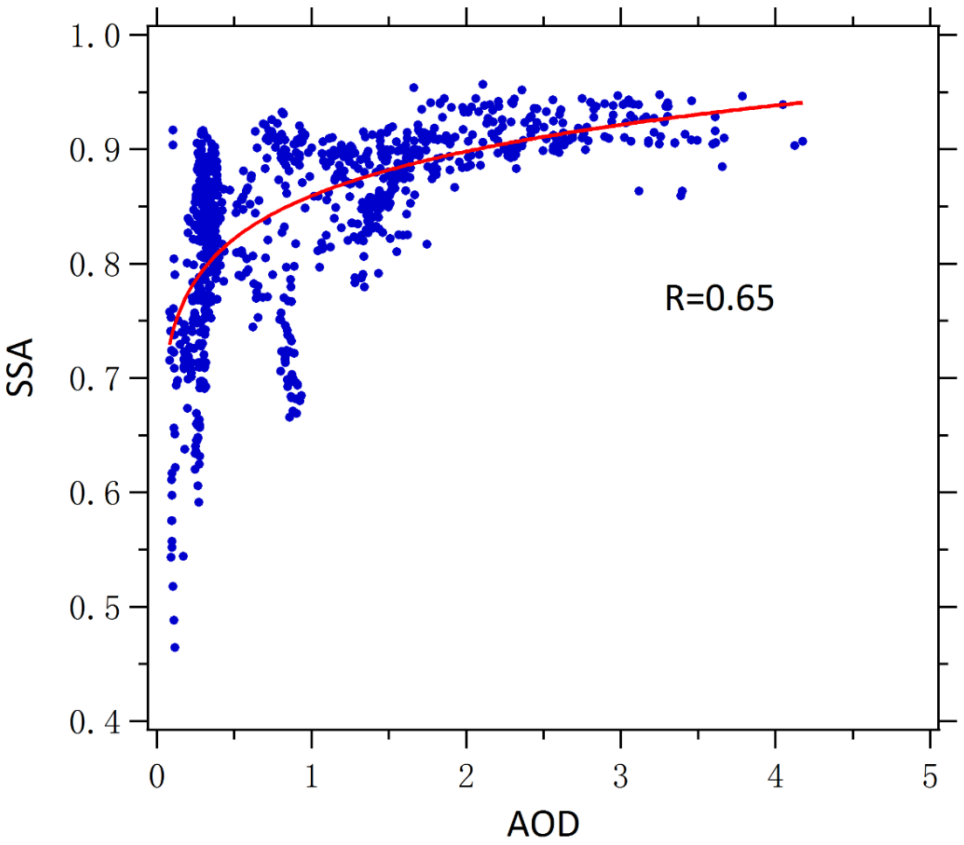

Figure 6. Correlation between SSA and AOD observed in August 2012.

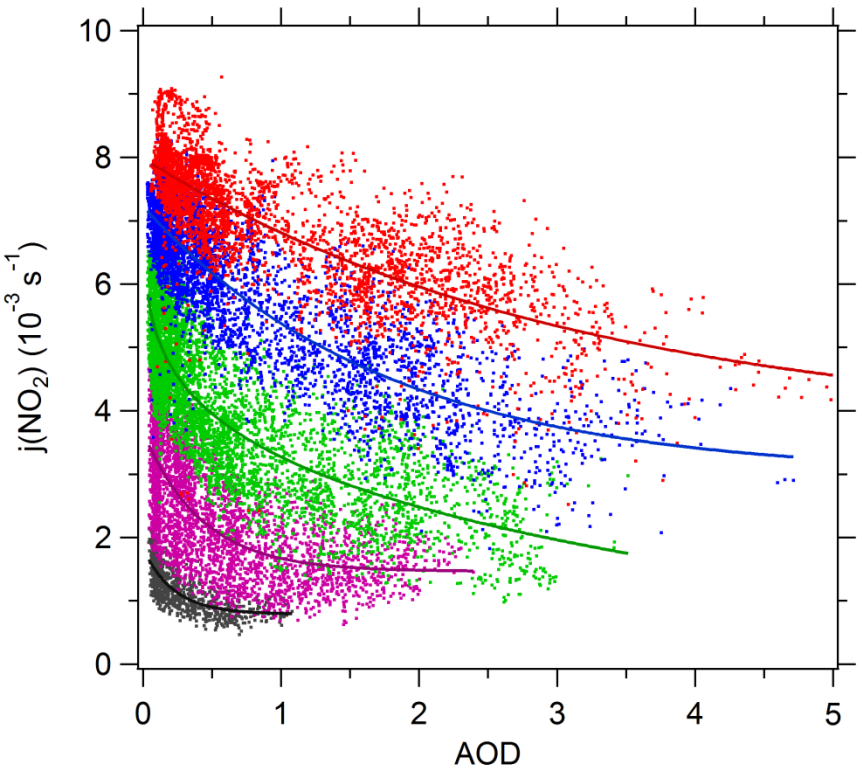

Figure 7. Dependence of $j(NO_2)$ on AOD at different SZA classes. The classes of cos(SZA) are 0–0.2 (black), 0.2–0.4 (purple), 0.4–0.6 (green), 0.6–0.8 (blue), and 0.8–1 (red).

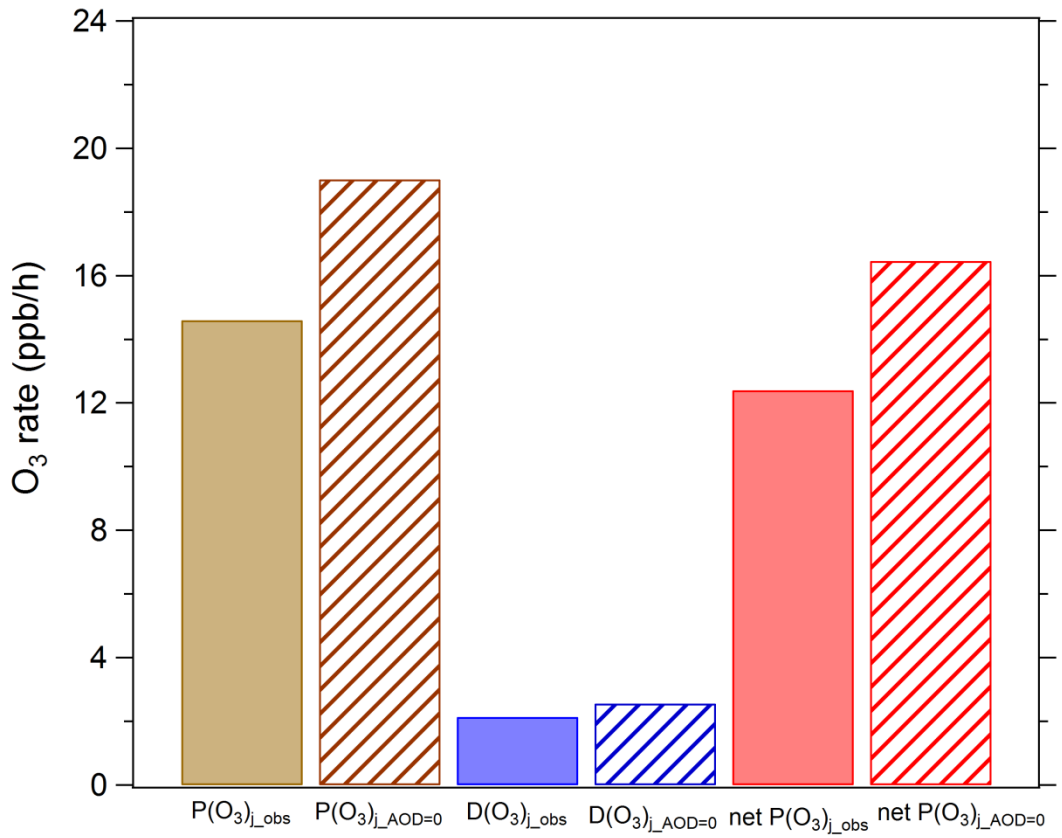

Figure 8. Average ozone production and loss terms in August 2012. $P(O_3)_{j\_obs}$, $D(O_3)_{j\_obs}$ and net $P(O_3)_{j\_obs}$ represents ozone production rate, ozone loss rate, and net ozone production rate under observed photolysis frequencies; $P(O_3)_{j\_AOD=0}$, $D(O_3)_{j\_AOD=0}$ and net $P(O_3)_{j\_AOD=0}$ represents ozone production rate, ozone loss rate, and net ozone production rate under calculated photolysis frequencies when AOD is equal to 0.

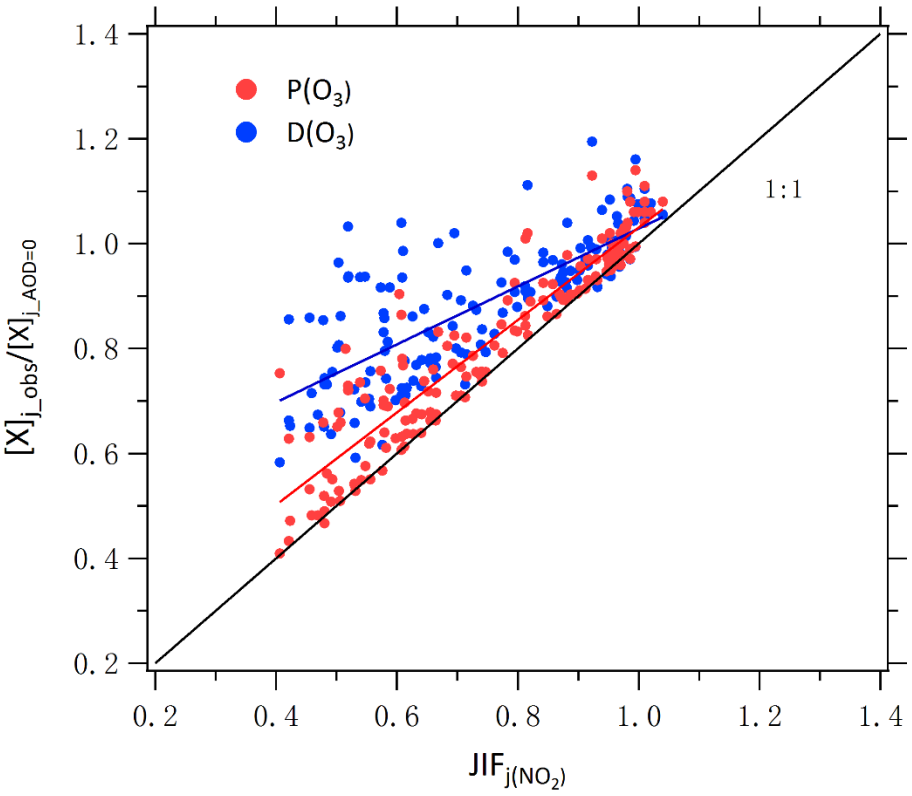

Figure 9. Correlation between $P(O_3)_{j\_obs}/P(O_3)_{j\_AOD=0}$ (or $D(O_3)_{j\_obs}/D(O_3)_{j\_AOD=0}$) and JIF of $j(NO_2)$.

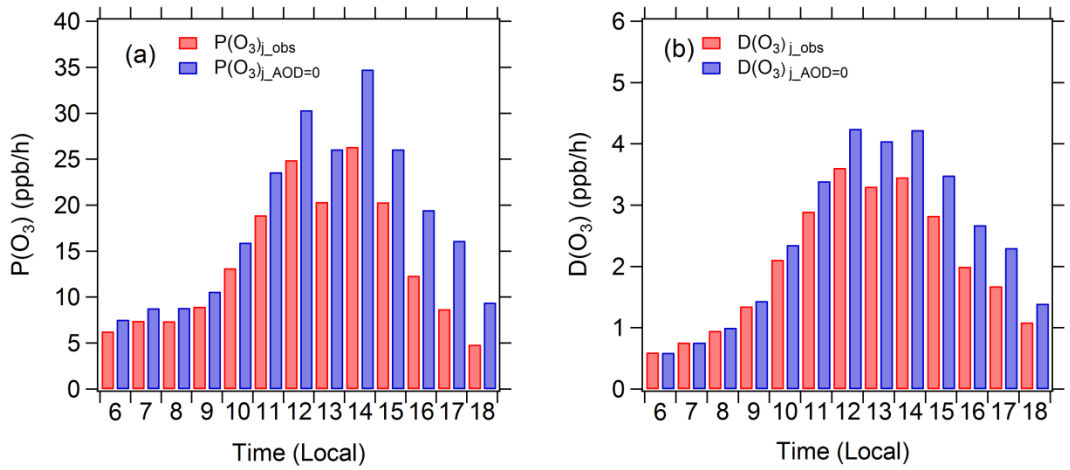

Figure 10. Diurnal profiles of mean $P(O_3)_{j\_obs}$, $P(O_3)_{j\_AOD=0}$, $D(O_3)_{j\_obs}$, and $D(O_3)_{j\_AOD=0}$.

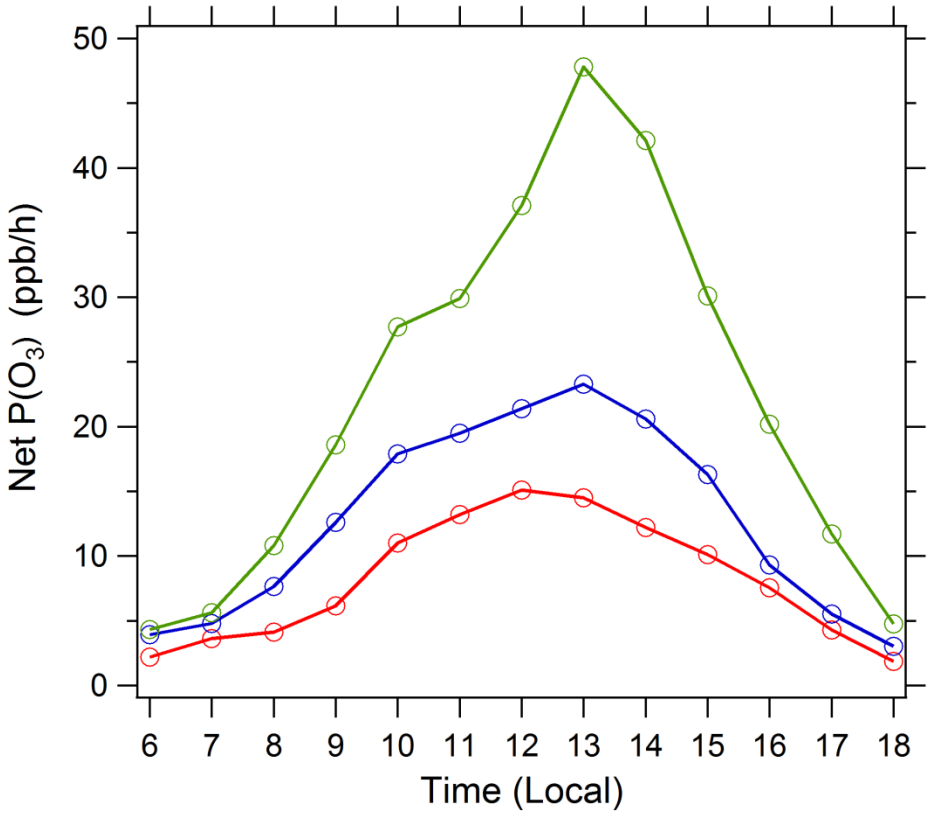

Figure 11. Diurnal profile of net $P(O_3)$ simulated by the box model. Three cases are displayed: (1) A day (red circles); (2) B day (blue circles); and (3) the photolysis frequencies of B day adjusted to the level of A day with other conditions unchanged (green circles).